TWO-PHASE FLOW PROPERTIES PREDICTION FROM SMALL-SCALE DATA USING PORE-NETWORK MODELING

C. Laroche, O. Vizika, Institut Français du Pétrole, G. Hamon, R. Courtial, TotalFinaElf

ABSTRACT

Mercury invasion performed on real porous media provides small-scale data characterizing pore-throat size distributions needed to calculate multi-phase relative permeabilities. For an accurate prediction of multi-phase transport properties other small-scale information on the rock structure and wettability may also be required. The objective of this work is to evaluate the prediction accuracy based on the interpretation of mercury invasion capillary pressure curves only.

A pore-scale modeling approach is used to model the multi-phase flow and calculate gas/oil relative permeability curves. The characteristics of the 3-D pore-network are defined with the requirement that the network model satisfactorily reproduces the P_c curve, the porosity and the permeability. A sensitivity study on the effect of the input parameters on the prediction of capillary pressure and gas/oil relative permeability curves is presented.

The simulations show that different input parameters can lead to similarly good reproductions of the experimental P_c, although the predicted K_r are somewhat widespread. This means that the information derived from a mercury invasion P_c curve is not sufficient to characterize transport properties of a porous medium. Other information is required to constrain the description of a rock sample and ensure a correct interpretation of the P_c curve. Comparison of predicted and experimental relative permeability curves gives insight into the critical parameters that need to be known in order to get more realistic predictions.

INTRODUCTION

A correct determination of relative permeabilities is of critical importance to reduce uncertainty on reserves and production forecasts. Experimental results have demonstrated a wide variability of relative permeability curves depending on the rocktype[1]. However a systematic study of the role that the different rocktype attributes play on the multi-phase flow transport properties is still missing.

For an accurate prediction of the transport properties of a porous medium small-scale data on the pore space geometry and topology are needed. Relative permeability prediction using pore networks replicating the microstructure of reconstructed porous media has already been reported[2]. However pore size data are most frequently obtained from mercury intrusion or retraction experiments, and using these easily obtained data to calculate transport properties is very attractive and challenging. Mercury invasion capillary pressure curves need to be interpreted in order to extract pore-throat radii distribution. A modeling of the pore space as well as important assumptions about its geometry and topology are

back to contents

hidden behind this interpretation. Network modeling to interpret mercury porosimetry drainage and imbibition curves taking into account particular pore geometry, surface roughness and pore-size correlations has been reported previously[3,4,5].

The objective of the present work is to evaluate the capability of network modeling to predict relative permeabilities through an adequate interpretation of mercury intrusion P_c curves. Different networks are built in a way to satisfy capillary pressure and standard petrophysical properties (porosity, permeability) determined experimentally. Gas/oil K_r curves are calculated at irreducible water saturation and compared to experimental data. A sensitivity study focusing on the effect of varying geometrical characteristics on the prediction of capillary pressure and gas/oil relative permeability curves is also presented.

PORE-SCALE MODELING

Network model construction

Pore space features

A network of the pore-and-throat type is a conceptual representation of a porous medium. Although it does not describe the exact morphology of a porous medium, it is able to take into account essential features of the pore space geometry and topology[6]. The network model developed and used in the present work respects the converging-diverging nature of pores, the multiple connectivity of the pore space, the distribution of pore sizes and the existence of pore space asperities or roughness.

The pore space is simulated as a three-dimensional cubic lattice formed by pore bodies (nodes) interconnected by pore throats (bonds). Pore bodies are made bigger than the pore throats, to ensure the converging-diverging nature of pores. The coordination number (bonds per node) can be varied. In the present work it is taken equal to 6. More details on the network model characteristics and construction are provided in a previous paper[7].

Mercury invasion data are used to extract pore-throat size distributions. Information on the pore-body size distribution can be obtained either from mercury retraction experiment or thin-section analysis. In constructing the network model, first, throat radii are randomly distributed according to the assumed distribution. Then in the absence of any other information about the pore-body size distribution, adjacent throat/pore-body correlation may be considered: in that case a fixed aspect ratio AR is defined between pore-body radii and the average of adjacent throat radii.

The presence of surface asperities and roughness is of high importance to model the flow of the wetting phase. For that reason, pore shape is considered to be either angular (triangular and square cross-sections respectively for pore-throats and pore-bodies), or to include fractal features to simulate pore-wall roughness as shown on Fig. 1. The throats form 45 degree angles to the flow direction in the horizontal plane. Periodic boundary conditions are used in the directions perpendicular to the inlet/outlet direction to minimize finite size effects.

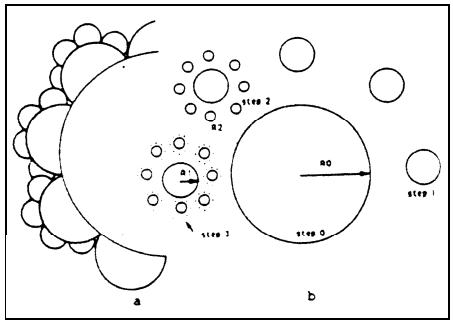

Figure 1 : Pore-wall fractal features (from Ref.8: Vizika and Lenormand, 1991)

Pore size distribution from mercury invasion capillary pressure curve

The determination of pore-throat size distribution in terms of a volume based density function from mercury invasion *Pc* curve is straightforward. Such a curve is a plot of the applied capillary pressure as a function of mercury saturation. The *Pc* vs. *S* curve is easily transformed into a *r* vs. *S* curve, where *r* is the threshold radius, if the capillary pressure across the hemispherical interface is defined using Young-Laplace equation :

$$Pc = \frac{2g\cos q}{r} \quad \text{……..……..……..…..……..(1)}$$

For mercury-air system, the interfacial tension g and the contact angle q are precisely known : $g = 480\,\text{mN/m}$ and $q = 140°$.

The volume based density function $f_v(r)$ is then given by:

$$f_v(r) = -\frac{dS}{dr} \quad \text{……..……..……..…..……..(2)}$$

The useful information to be extracted from the mercury invasion curve for the construction of the network model is the number based throat size frequency. To determine the number based density function $f_n(r)$ certain assumptions have to be made:

- Radii r calculated from the capillary pressure values correspond to the threshold radii to invade pore bodies of radius $R \propto r$.
- All the porous volume is contained in the pore-bodies; the porous volume contained in the pore-throats is negligible. When a fractal surface roughness is assumed, the ratio S_f of the volume contained in the fractal tubes to the pore-throat total volume is: $S_f = p^{\frac{D_L - 2}{D_L - 1}}$. For common values of the fractal dimension D_L the fractal volume remains of the order of magnitude of the main pore-throat volume.
- The elementary volume of a pore-body of radius $R \propto r$ is proportional to its threshold radius to a certain power l, i.e. $v(r) \propto r^l$.

The relationship between volume and number based density function is then given by:

$$f_n(r)\frac{v(r)}{\bar{v}} = f_v(r) \quad \text{……..……..……..…..……..(3)}$$

where $\bar{v}$ is the average elementary volume of a pore, verifying $\bar{v} \propto \overline{r^l}$.

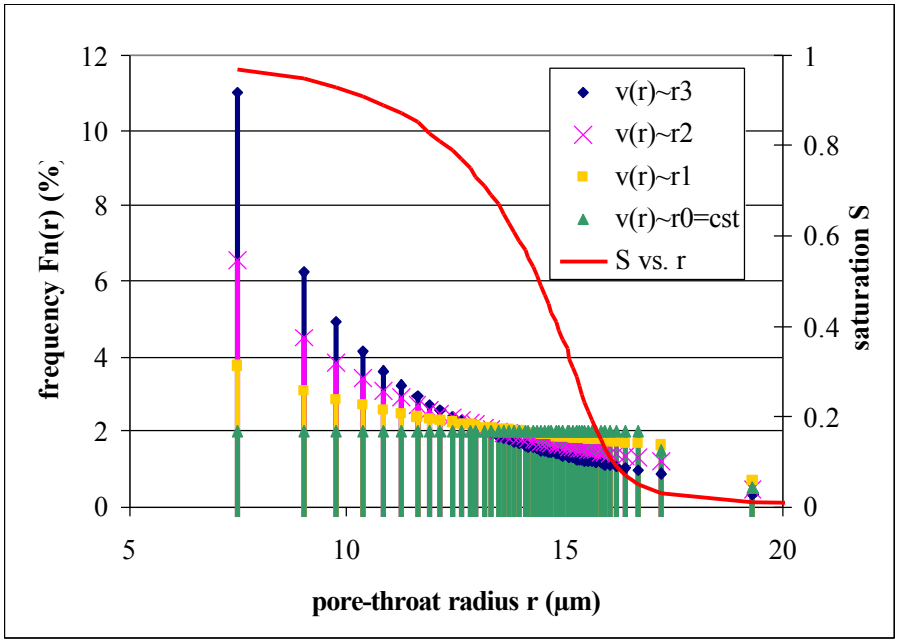

Figure 2 : Mercury saturation vs. pore-throat radius curve from mercury invasion Pc curve and the subsequent pore-throat radius distributions.

No information is directly extracted from the mercury invasion P_c curve concerning the pore-body size distribution. However, if the pore-body dimension is assumed to be proportional to its threshold radius $R \propto r$, the pore-body size distribution will give automatically the pore-throat size distribution. The proportionality coefficient is fixed by the aspect ratio *AR*. It is to be noted that the pore-body dimension can be independent from the threshold radius when the pore-body volume is supposed to be constant: $v(r) \propto r^l$ with $l = 0$. In such a case, the aspect ratio is defined as the ratio of the constant pore-body radius to the average pore-throat radius. An example of a mercury saturation vs. pore-throat radius curve from mercury invasion P_c curve and the subsequent pore-throat radius distributions calculated assuming different pore body volume relationships $v(r) \propto r^l$ is given in Figure 2. The distributions are expressed in terms of frequency $F_n(r)$ defined from the number based density function $F_n(r) = |f_n(r)dr| = \left|\frac{\bar{v}}{v(r)}dS\right|$. In the simulations presented here each pore body is assumed to be accessible by pore-throats (six) of identical radii. This implies that pore-throats, which by definition are linking two pore-bodies, do not have a constant section and are defined by two radii.

Calculation of petrophysical parameters
Network invasion methodology

Capillary pressure curves are obtained by simulating quasi-static displacement: an increasing pressure is applied on the injected fluid, while the pressure of the fluid in place is kept constant. During quasi-static displacement, viscous pressure gradients are negligible, and the pressure of each phase is constant everywhere within the network.

For the calculation of a mercury capillary pressure curve, mercury invasion in an empty network is simulated. Mercury is the non-wetting phase, and drainage mechanism dominates similarly to a capillary-controlled gas-oil displacement. Gas-oil quasi-static displacement is simulated after a first water-oil displacement (invasion of oil in a water saturated network) to reach irreducible water saturation.

Drainage involves piston-like displacements : for a given applied pressure difference $P_{Cab} = P_a - P_b$ between the injected phase a and the fluid in place b, the invasion of a given throat or pore occurs if P_{Cab} exceeds the threshold pressure of the throat or pore. Drainage displacements are therefore controlled by throat sizes, since the curvature in a pore body is smaller than the curvature in a throat. For that same reason, when a throat is invaded, the contiguous pore body is automatically invaded. For each applied capillary pressure level, all the possible invasions in the accessible throats/pores are performed provided that the displacement criterion is satisfied.

Wetting and Non-Wetting phase Saturation

The main contribution to the local saturation in the pore space comes from the bulk phase. However when two or three phases are present within a pore, the saturation of the wetting phase occupying the corners or the fractal features may not be negligible and needs to be accounted for. The saturations of the different phases depend on the relative positions of the interfaces present in the pore, and therefore, depend on the capillary pressures between the different phases, which fix the interface radius of curvature.

For instance, in a fractal geometry, for the highest P_c values, the wetting phase occupies the smallest fractal tubes, and the non-wetting phase invades the largest fractal tubes. Quantitative expression to evaluate the local saturation of the different phases can be found elsewhere[7,9].

Relative Permeability calculation

Gas-oil relative permeability curves are calculated during gas-oil quasi-static displacements when capillary equilibrium is reached. Flow within each phase is simulated by applying a macroscopic pressure gradient ΔP across the network of length L. If Q_a is the flow rate and m_a the viscosity of phase a, its relative permeability is calculated as:

$$K_{ra} = \frac{Q_a m_a L}{AK\Delta P} \quad \text{.....(4)}$$

where K is the permeability, and A the cross-section of the porous medium.

The network model uses an electrical analog to calculate the fluid flow of each phase spanning the network: voltage is replaced by pressure, electrical conductance by hydraulic conductance. Under laminar flow conditions the relationship between pressure drop and fluid flux in the network is linear. The local flow rate between pore i and neighboring pore j is defined as:

$$q^a_{ij} = g^a_{ij} (P^a_i - P^a_j) \quad \text{.....(5)}$$

for a particular fluid a, existing in a throat as bulk phase or film phase. g^a_{ij} is the local conductance of the considered phase between pores i and j. Quantitative expression for the local conductance of the different phases can be found in previous work for both the fractal and the angular geometry[7,9]. In each pore i the continuity equation requires that:

$$\sum_j q^a_{ij} = 0 \quad \text{.....(6)}$$

The problem for a certain flow situation is reduced to a system of linear algebraic equations, the solution of which gives the pressure of each phase in the pores. The solution of the system is obtained using a biconjugate gradient method[10].

RESULTS AND DISCUSSION

Three experimental cases have been investigated. The studied cores where three sandstones, with very different porosities and permeabilities. As seen on Table 1, Core A presents a very high porosity and permeability. Cores B and C have similar porosities, around 20%, typical of sandstone, but very different permeabilities: Core C is a low permeability rock. All three cores were water-wet. The oil was assumed to spread on water in the presence of gas.

Capillary pressure curves

Mercury invasion experiments were performed on these three cores to obtain capillary pressure curves, from which pore size distributions were extracted. The experimental P_c curves obtained from these experiments are very different (Figure 3).

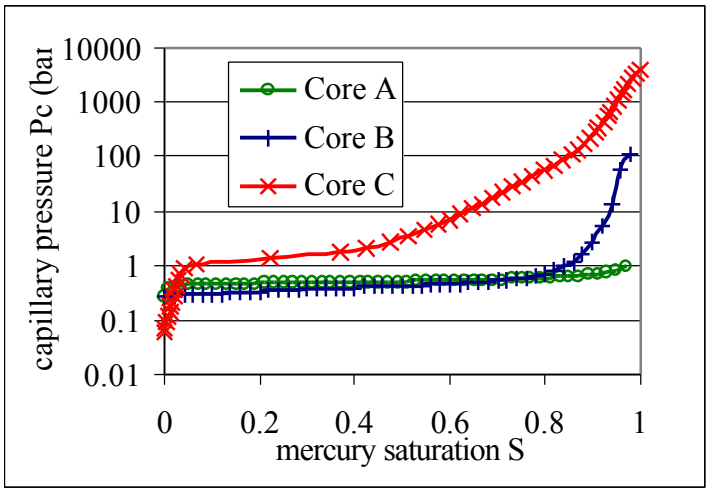

Figure 3: Experimental Pc curves for Cores A, B and C from mercury invasion experiments.

	F, %	K, mD
Core A	**43.0 –43.3**	**5400-8800**
Core B	**21.1-21.9**	**1827-2700**
Core C	**19.6**	**6.3**

Table 1: Core characteristics

Core A presents a plateau, without any spreading of the capillary pressure values around the plateau value. Core B also presents an important plateau, but the capillary pressure starts increasing significantly for mercury saturations above 80%. No plateau is apparent on the Core C curve: the curve exhibits an important spreading of the capillary pressure

values, with an early increase starting when only 40% of the pore space is invaded by mercury. From those different behaviors, we will try to extract sufficient information to describe the cores and to predict the corresponding relative permeabilities.

The characteristics of the different networks constructed for the three studied cases are given in Tables 2 to 4. The corresponding P_c curves for all three cases are given in Fig. 4. It is seen that for the different assumptions on the pore geometry, different pore size distributions are extracted from the same experimental data. All these distributions satisfy the same capillary pressure curve rather satisfactorily. In fact the aspect ratio and the periodicity length (node to node distance) are used as adjustable parameters to fit the porosity and permeability experimental data.

Case A: Different scenarios $v(r) \propto r^l$ have been tested for λ varying between 0 and 3. The coefficient of the expression is adjusted as well as the AR and the periodicity length, as it can be seen in Table 2. The porosity and permeability are very satisfactorily given. All configurations, correlated and uncorrelated, satisfy the experimental P_c (Figure 4).

Case B: On this sample the following problem has been encountered. If a correlation between body and throat sizes is assumed ($\lambda \geq 1$), the obtained size distribution is not physically realistic. In fact a disproportionately high number of too small pores is generated even for a weak body-throat correlation ($\lambda = 1$). The retained solutions, presented in Table 3, are only the ones for $\lambda = 0$, or $\lambda = 1$ for r>5μm and uncorrelated for r < 5μm. In the model B4 an uncorrelated throat-body size distribution has been combined with a fractal pore surface for the pore-throats. The linear fractal dimension, D_L, has been taken equal to 1.6 (surface fractal dimension 2.6). It has been derived from the mercury capillary pressure curve using the following correlation[8]:

$$P_c \propto S_W^{\frac{1}{D_L - 2}} \quad \text{.....(7)}$$

This value for D_L compares favorably with the range of values reported for natural sandstones and measured in SEM studies[11].

Case C: Exactly the same problems are present for case C. An unrealistic pore size distribution is obtained for any body-throat correlation. Even for λ=1 the majority of pore-throats have sizes less than 0.01μm (Figure 5). As in case B the most realistic distributions have been obtained for completely uncorrelated body-throat sizes (λ=0) or for a weak correlation (λ=1) down to 5μm pore size and uncorrelated below. Finally both options are comparable to each other since only a few pores larger than 5μm exist.

Relative permeability curves

Gas-oil relative permeabilities at irreducible water conditions (S_{wi}) have been calculated for the three cores and for all the different representations listed in Tables 2 to 4. The results are presented in Figures 6a, 6b & 6c both in logarithmic and linear coordinates. No experimental measurements were available for Core A. It is seen that all five representations give comparable values for the wetting phase Kr at relatively high

saturations. For low saturations the obtained values diverge. This is understandable since at low wetting phase saturation its relative permeability depends strongly on the phase

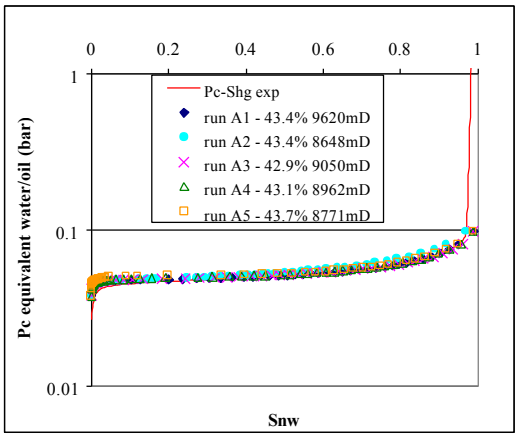

Core A

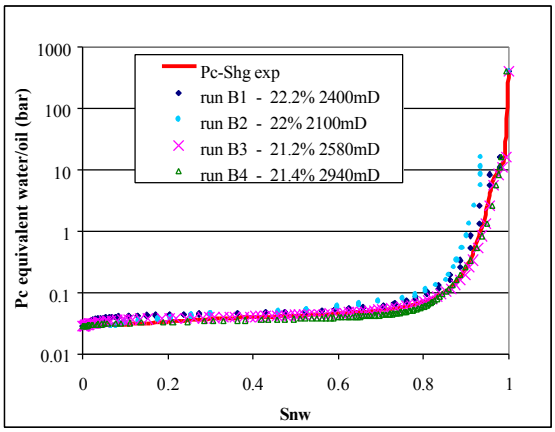

Core B

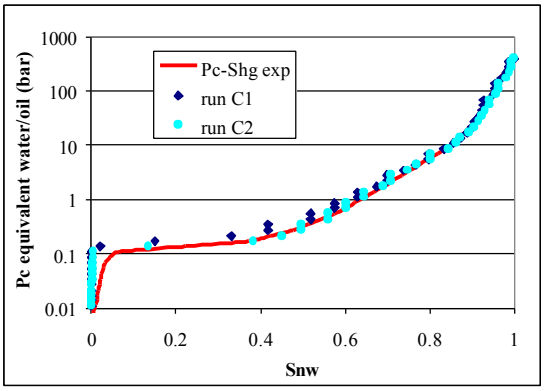

Core C

Figure 4 : Comparison between simulated and experimental capillary pressure curves

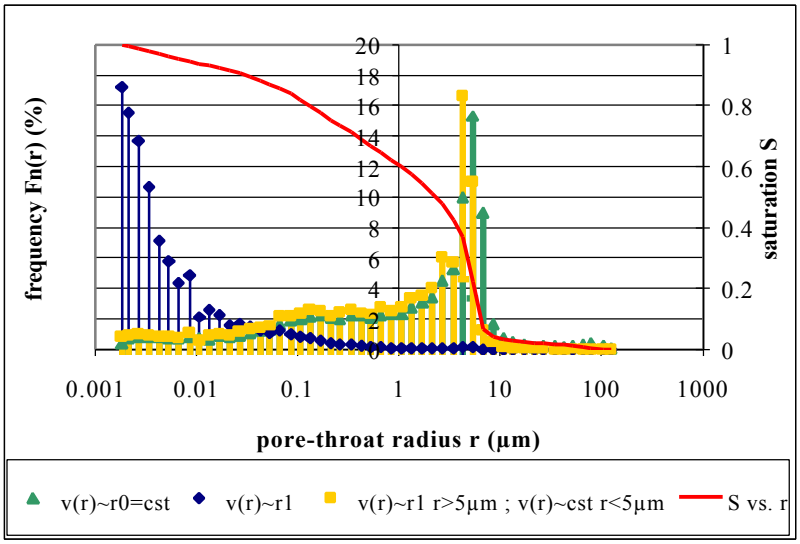

Figure 5 : Mercury saturation vs. pore-throat radius curve for core C and the subsequent pore-throat radius distributions calculated assuming different pore body volume relationships $v(r) \propto r^{l}$.

		F, %	K, mD
Experimental values : Core A		**43.0 -43.3**	**5400-8800**
Run A 1	Uncorrelated throat-body sizes : $v(r)=cst=0.7*86^3 \propto r^0$ AR=3. 0 - L= 105µm	**43.4**	**9623**
Run A 2	Uncorrelated throat-body sizes : $v(r)=cst=0.7*55^3 \propto r^0$ AR=1.5 - L= 71µm	**43.4**	**8648**
Run A 3	Correlated throat-body sizes : $v(r)= 5250*r \propto r^1$ AR=3.0 - L= 104µm	**42.9**	**9053**
Run A 4	Correlated throat-body sizes : $v(r)= 60*r^2 \propto r^2$ AR=3. 0 - L= 100µm	**43.1**	**8962**
Run A 5	Correlated throat-body sizes : $v(r)= 0.7*r^3 \propto r^3$ AR=3. 0 - L= 95µm	**43.7**	**8771**

Table 2: Pore geometry assumptions for Core A , and simulated porosity and permeability.

		F, %	K, mD
Experimental values : Core B		**21.1-21.9**	**1827-2700**
Run B 1	Correlated throat-body sizes for r>5µm : v(r)∝r Uncorrelated throat-body sizes for r<5µm : v(r)=cst, L= 17µm	**22.2**	**2400**
Run B 2	Density function $f_n = 0.066* r^{-0.5}$ Correlated throat-body sizes for r>5µm : v(r)∝r Uncorrelated throat-body sizes for r<5µm : v(r)=cst, L= 18µm	**22.0**	**2100**
Run B 3	Uncorrelated throat-body sizes : v(r)=cst AR=5.5 - L= 243µm	**21.2**	**2580**
Run B 4	Uncorrelated throat-body sizes : v(r)=cst AR=3.0 - L= 155µm - Fractal pore throat DL=1.6	**21.4**	**2940**

Table 3: Pore geometry assumptions for Core B , and simulated porosity and permeability.

		F, %	K, mD
Experimental values : Core C		**19.6**	**6.3**
Run C 1	Uncorrelated throat-body sizes : v(r)=cst	**19.9**	**5.4**
Run C 2	Correlated throat-body sizes for r>5µm : v(r)∝r Uncorrelated throat-body sizes for r<5µm : v(r)=cst	**19.7**	**5.2**

Table 4: Pore geometry assumptions for Core C , and simulated porosity and permeability.

continuity, which in turn depends on the geometric characteristics of the pore network. For the non-wetting phase the obtained values are all comparable to each other except for run A5 where a strong throat-body size correlation exists.

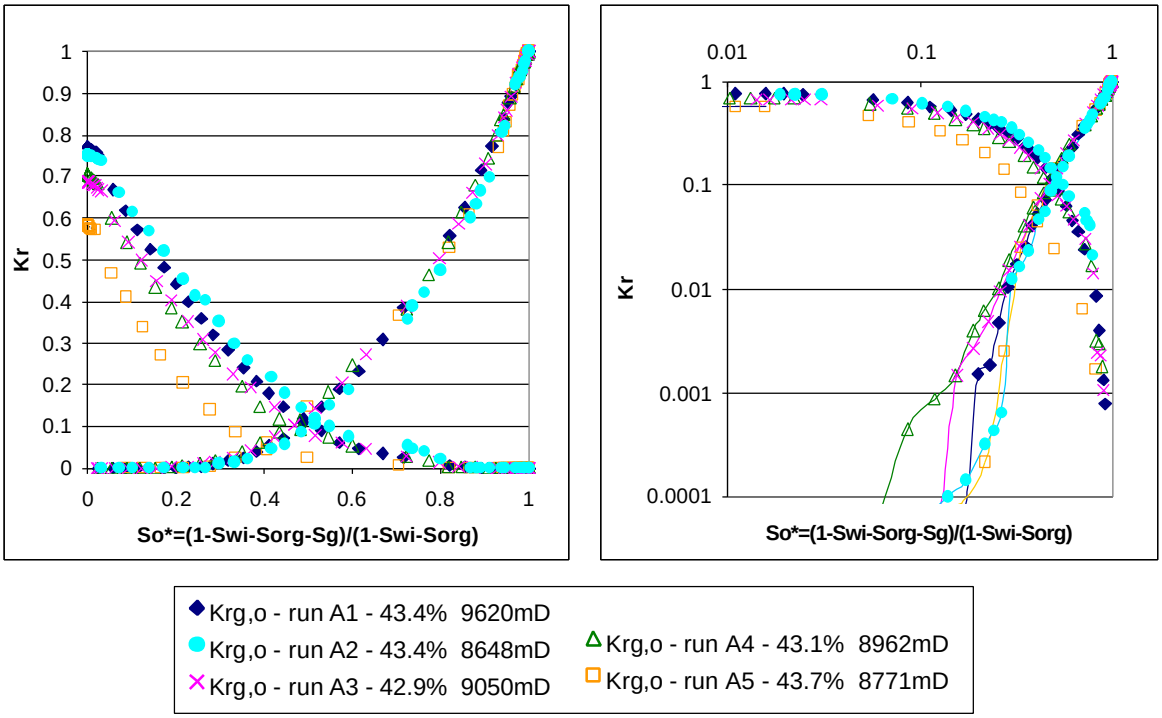

Figure 6a : Core A – comparison between simulated gas and oil relative permeabilities at Swi for different pore geometry (see table 2)

For Cores B and C the experimentally measured values are also given for comparison purposes (Figs 6b&c). For Core B and for the oil phase a rather satisfactory agreement is observed between experimental results and representations B1 and B2. Runs B3 and B4 underestimate somewhat K_{ro} for intermediate oil saturations. Run B3, characterized by high AR and L values, underestimates severely K_{ro} at low oil saturations. This may be due to the fact that in these cases the oil, as wetting phase, circulates inside very thin throats of reduced conductivity (fractal roughness or film flow inside thin throats). For the same cases and probably for the same reasons K_{rg} is slightly overestimated. The best agreement is obtained with a throat-body correlation above 5μm and uncorrelated sizes below 5μm.

For Core C two experimental measurements were available: one from a centrifuge experiment and another from displacement interpreted with JBN method. The two simulations, run with completely uncorrelated throat-body sizes and with a correlation only above 5μm, agree rather well with each other and with the experimental results. The differences are smaller than the spread of the experimental measurements themselves.

CONCLUSIONS

Network modeling has been used to interpret mercury porosimetry data and to construct pore networks satisfying capillary and standard petrophysical properties of real rocks. Gas/oil relative permeabilities in the presence of irreducible water have been calculated in these networks and compared to experimentally determined curves.

The simulations show that different input parameters for the pore structure can lead to similarly good reproductions of the experimental capillary pressure, while rather different

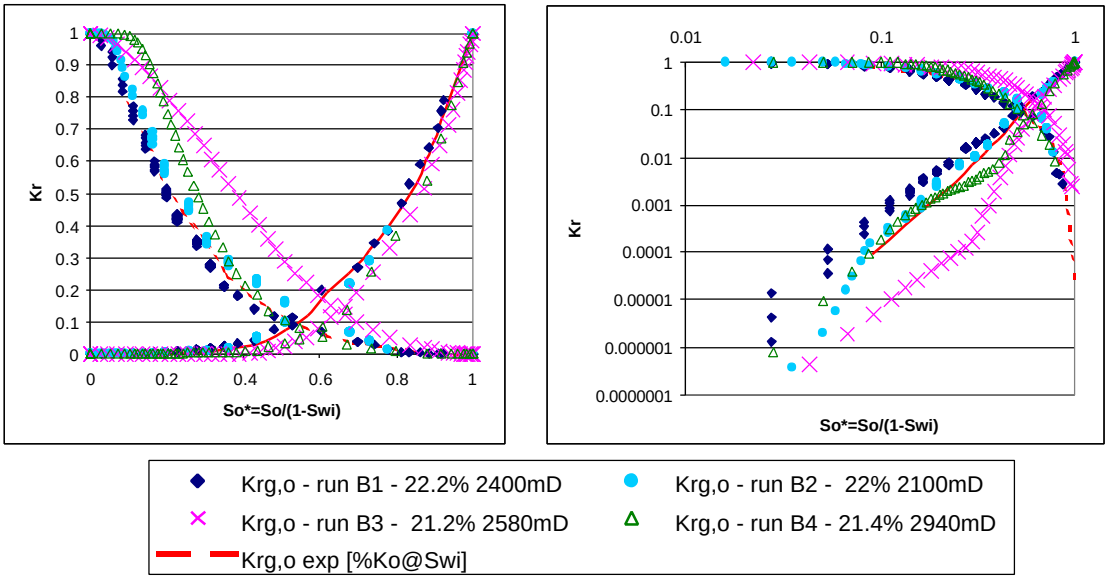

Figure 6b : Core B – comparison of gas and oil relative permeabilities at Swi obtained by experiment and simulations for different pore geometry (see table 3)

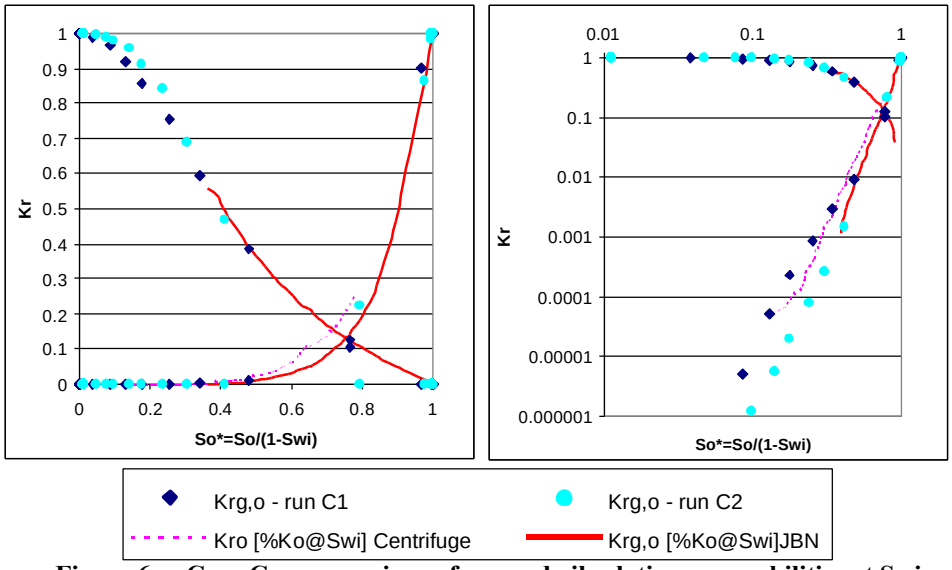

Figure 6c : Core C – comparison of gas and oil relative permeabilities at Swi obtained by experiment and simulations for different pore geometry (see table 4)

relative permeability values are obtained. These differences are more accentuated for the wetting phase relative permeability at low saturations where the geometry of the pores and pore-walls as well as the assumptions about the hydraulic continuity and conductivity are expected to be most important. More quantitative information on the wall roughness and the node/bond aspect ratio would be necessary to better constrain the problem.

The existence of a correlation between node and bond sizes plays also an important role. The comparison with experimentally determined K_r, which is rather satisfactory, indicates that in narrow pore size distributions node volume and bond radius seem correlated while in broad pore size distributions they would be uncorrelated.

NOMENCLATURE

f_v = volume based density function
f_n = number based density function
g = conductance
q = flow rate
r = throat radius
$\overline{v}$ = average elementary volume
g = interfacial tension
q = contact angle
m = viscosity
f = porosity
A = network cross-sectional area
D_L = linear fractal dimension
K = permeability
K_r = relative permeability
L = network length
P = pressure in the center of a pore
P_C = capillary pressure
Q = flowrate through the network
R = pore body radius
S = saturation
S_f = ratio of fractal volume to pore-throat total volume
ΔP = macroscopic pressure drop applied across the network

Subscripts

a, b = fluid in place
i = pore i
ij = between neighboring pores i and j
g,o = gas, oil phase

REFERENCES

1 Hamon G; Pellerin F M 'Evidencing Capillary Pressure And Relative Permeability Trends For Reservoir Simulation', SPE 38898, (1997) *SPE Annual Technical Conference and Exhibition*, San Antonio, Texas, USA, Oct. 5-8

2 Øren, P.E., Bakke, S., Arntzen, O.J.: "Extending Predictive Capabilities to Network Models", paper SPE 38880 (1997) *SPE Annual Technical Conference and Exhibition*, San Antonio, Texas, USA, Oct. 5-8.

3 Tsakiroglou C D, Payatakes A C: 'Effects Of Pore-Size Correlations On Mercury Porosimetry Curves', *J Colloid Interface Sci*, (1991), **146**, 2, 479-494

4 Tsakiroglou C D, Payatakes A C : 'Pore-Wall Roughness As A Fractal Surface And Theoretical Simulation Of Mercury Intrusion/Retraction In Porous Media', *J Colloid Interface Sci*, (1993), **159**, 2, 287-301

5 Tsakiroglou C D; Kolonis G B; Roumeliotis T C; Payatakes A C : 'Mercury Penetration and Snap-Off in Lenticular Pores', *J Colloid Interface Sci ,* (1997) **193**, 2, 259-272

6 Thauvin, F., Mohanty, K.K.: 'Network modeling of non-Darcy Flow Through Porous Media', *Transport in Porous Media* (1998) **31**, 19-37

7 Laroche, C., Vizika, O., Kalaydjian, F: 'Network modeling as a tool to predict three-phase gas injection in heterogeneous wettability porous media', *Journal of Petroleum Science and Engineering*, (1999) **24** , 155-168

8 Vizika O., Lenormand R. "Flow by film of the wetting phase in a porous medium and its role on the gravity drainage process", *presented at the IEA 12th International Workshop and Symposium*, Bath, UK, 28-30 October, 1991

9 Laroche, C ,'Capillary pressure and relative permeability curves in mixed-wet media using Network modeling', Proceedings, *6th International Symposium on Evaluation of Reservoir Wettability and its Effect on Oil Recovery*, 27-28 septembre 2000, Socorro, NM, USA.

10 Press, W.H., Flannery, B.P., Teukolsky, S.A., Vetterling, W.T.: *Numerical Recipes: The Art of Scientific Computing* Cambridge University Press, Cambridge (1989).

11 Katz, A.J. , Thompson, A.H., 'Fractal Sandstone Pores : Implications for Conductivity and Pore Formation', *Phys. Rev. Lett.,* (1985) , 54, 1325-1328.

back to contents